Digest Journal of Nanomaterials and Biostructures Vol. 19, No. 4, October-December 2024, p. 1561-1575

Research on $PbTiO_3$ nanoparticles optimized mesoporous layer for perovskite solar cells

Y. H. Zhang[a], J. Y. Li[b], J. W. Li[b], H. J. Tao[b], C. X. Zhang[a,*]
[a]*School of Materials Science and Engineering, Nanjing Institute of Technology, Nanjing 211167, China*
[b]*College of Materials Science and Technology, Nanjing University of Aeronautics and Astronautics, Nanjing 211106, China*

Organic-inorganic hybrid perovskite solar cells have garnered significant attention due to their facile fabrication process and high photovoltaic conversion efficiency. The electron transport layer plays a crucial role in the carrier separation mechanism of perovskite solar cells, making it a focal point for enhancing cell performance. In this study, $PbTiO_3$ was introduced into TiO_2 mesoporous layers by modification and doping in order to optimize cell performance. Initially, the use of $PbTiO_3$-modified mesoporous layers revealed issues such as non-uniform modification layers, low film coverage rates, and reduced light transmittance. These issues hindered the ability of $PbTiO_3$ to facilitate carrier separation and resulting in suboptimal optimization effects. However, by utilizing $PbTiO_3$-doped mesoporous layers for optimizing cell performance, we observed improved quality and higher light transmittance in the perovskite films. As a consequence of the improved carrier separation achieved by $PbTiO_3$, the efficiency of the solar cell has been enhanced to 5.51%.

(Received July 13, 2024; Accepted October 19, 2024)

Keywords: Perovskite solar cells, Electronic transport layer, Ferroelectric material, Modification layer, Doping

1. Introduction

The demand for new energy sources increases year after year with the development of human society. Among the new energy sources, solar energy has had a profound impact on human life and has become the focus of research [1]. Solar cells have undergone three generations of development with the photoelectric conversion efficiency increasing from 3.8% to 26% [2]. Organic-inorganic hybrid perovskite solar cells have attracted considerable attention due to advantageous properties, including a direct band gap, high light absorption coefficient, low exciton binding energy, long exciton and carrier diffusion distance, low cost, a simple preparation process and high photoelectric conversion efficiency [3]. The electron transport layer plays a key role in separating charge carriers in perovskite solar cells, and optimizing this layer can effectively improve the photoelectric conversion efficiency [4].

* Corresponding author: zhangcxnuaa@njit.edu.cn
https://doi.org/10.15251/DJNB.2024.194.1561

Ferroelectric materials have attracted significant attention due to their capability of generating depolarizing electric fields and facilitating the separation of charge carriers. Tomas et al. proposed the utilization of ferroelectric metal oxide $PbZrTiO_3$ as an electron transport layer, whereby the oxygen vacancy-induced defect dipole of $PbZrTiO_3$ can facilitate carrier separation [5]. Feng et al. employed $BaTiO_3/TiO_2$ composite particles as the photoanode for dye-sensitized solar cells. The $BaTiO_3$ ferroelectric dipole to suppress carrier recombination near TiO_2 surface, thereby enhancing electron mobility and improving the photogenerated current density and filling factor of the cell [6]. Therefore, this study employs the depolarization electric field generated by ferroelectric materials [7] to effectively separate photo-generated electron-hole pairs and optimize the TiO_2 mesoporous layer. In order to achieve these objectives, it is necessary to select appropriate ferroelectric materials are selected based on the following criteria: (1) n-type semiconductor properties; (2) band alignment with TiO_2 and perovskite materials to form a trapezoidal band structure; (3) high conductivity; (4) strong spontaneous polarization intensity; (5) low cost. In accordance with the aforementioned conditions, this paper selects $PbTiO_3$ ferroelectric material to optimize the perovskite solar cell. [8].

Currently, the synthesis of $PbTiO_3$ nanoparticles is conducted via two principal methods: the sol-gel method and the hydrothermal method [9-11]. Among these methods, the hydrothermal method allows for the preparation of nanoparticles with a fine particle size, complete crystallization, no agglomeration, and high activity at lower temperatures [10]. Therefore, this study employs the hydrothermal method to synthesize $PbTiO_3$ nanoparticles. Previous studies have demonstrated that the introduction of a modified layer and doping between the perovskite film and electron transport layer can significantly enhance the carrier separation rate at the interface [12,13]. This study also employs these two approaches to optimize the electron transport layer, while investigating the impact of modified layer thickness and doping mass fraction on the cell's carrier separation. Ultimately, the introduction of $PbTiO_3$ into the TiO_2 mesoporous layer by doping has been demonstrated to enhance the photovoltaic conversion efficiency of the perovskite solar cell by up to 5.51%.

2. Experimental

2.1. Experimental drugs

Isopropyl alcohol, isopropyl titanate, lead iodide, titanium tetrachloride, lead acetate trihydrate, chlorobenzene (Aladdin Reagent Co., LTD.); anhydrous ethanol, ethyl cellulose, graphite powder (Sinopharm Group Chemical Reagent Co., LTD.); zinc powder, concentrated hydrochloric acid (Nanjing Chemical Reagent Co., LTD.); dimethylformamide, dimethyl sulfoxide (Sigma-Aldrich); pine oleanolic acid (Shanhai Jiuyue Chemical Reagent Co., LTD.); FTO glass (Yingkou Opivet New Energy Technology Co., LTD.); carbon black (Japanese daily chemical brand Co., LTD.); methyl iodinated amine (Xi 'an Baolai Photoelectric Technology Co., LTD.); TiO_2 slurry (Jiangsu Yanchang Sanglai New Energy Co., LTD.), the above reagents are further purified.

2.2. Experimental apparatus

Electronic precision balance (FA2004B, Shanghai Jingke Tianmei Scientific Instrument Co., Ltd.); Heat collector type constant temperature heating magnetic stirrer (DF-101S, Gongyi Yuhua Instrument Co., Ltd.); Numerical control ultrasonic cleaner (KH3200DE, Kunshan Hechuang

Ultrasonic Instrument Co., Ltd.); Electric heat constant temperature blast drying oven (DGG-9140B, Shanghai Senxin Experimental Instrument Co., Ltd.); Transfer gun (Dalong Xingchuang Experimental Instrument Co., Ltd.); Planetary ball mill (QM-3SP4, Nanjing Nanda Instrument Co., Ltd.); Rotary coating instrument (EZ4, Jiangsu Lebo Scientific Instrument Co., Ltd.); Muffle furnace (NBD-M1200, Norbert Material Technology Co., Ltd.); Vacuum drying oven (DZF-6020MBE, Shanghai Boxun Industrial Co., Ltd.); Constant temperature magnetic stirrer (IKA C-MAG HS 4 AICA Instrument Equipment Co., Ltd.); Annealing platform(V-2020T Dongguan Weiteike Automation Technology Co.Ltd.).

2.3. Preparation of perovskite solar cells

FTO conductive glass cleaning: The FTO conductive glass (25mm×20mm) was etched with zinc powder and hydrochloric acid, followed by ultrasonic treatment using washing powder water, glass cleaning solution, anhydrous ethanol, and distilled water for 15 minutes each. Finally, the glass was dried with a hot hair dryer for later use.

Dense layer preparation: The precursor solution A was prepared by slowly adding 370 μL of isopropyl titanate to 2,530 μL of isopropyl alcohol and stirring until homogeneous. Solution B was obtained by slowly adding 35 μL of 2M hydrochloric acid to 2,530 μL of isopropyl alcohol and stirring evenly. Subsequently, solution B was gradually added to solution A with continuous stirring, resulting in the formation of precursor solution C. After spin-coating on the FTO substrate for 60s at a speed of 2000rpm, precursor solution C was transferred to a muffle furnace and heated at a temperature of 500 °C for a duration of 30 minutes following the completion of spin-coating. Finally, it was removed after cooling for further use.

$PbTiO_3$ slurry Preparation: The $Pb(OAc)_2 \cdot 3H_2O$ was dissolved in anhydrous benzyl alcohol and stirred until it became transparent. Subsequently, tetraisopropyl titanate and oleic acid were added separately and stirred. The resulting solution was then transferred to a reaction kettle and maintained at various temperatures for 2 hours to yield white gelatinous products. Finally, the precipitate was sequentially washed three times with ethanol followed by toluene.

Mesoporous layer preparation: The commercial TiO_2 slurry and anaqueous ethanol were prepared into a mesopore layer spin-coating slurry with a mass ratio of 1:7, and then the slurry was spin-coated on the dense layer for 30 s at 3000 rpm. After spin-coating, the slurry was transferred to the Muffle furnace for annealing at 500 ℃ for 30 min. After cooling, the dispersion liquid of $PbTiO_3$ slurry was spin-coated on the surface of the mesopore layer for 30s at 3000 rpm. And then heating at 500℃ for 30 min as the $PbTiO_3$ modification layer. $PbTiO_3$ doped mesoporous layer is prepared by mixing $PbTiO_3$ paste with mesoporous layer paste and spinning coating on dense layer.

modified layer Preparation: First, 880 μL of titanium tetrachloride was added to a frozen ice cube in 200mL of distilled water, and the ice cube was dissolved in a water bath at 50 °C to prepare a solution of titanium tetrachloride. Subsequently, the prepared substrate was immersed in the aqueous solution of titanium tetrachloride and maintained at 70 °C for 30 minutes. Afterwards, the substrate was removed and sequentially washed with water and anhydrous ethanol.

perovskite layer Preparation: Add 1.2 mmol CH_3NH_3I and 1.2 mmol PbI_2 into 0.915 mL DMF and 0.085 mL DMSO mixed solution and stir until the transparent and clear yellow solution, then spin the perovskite precursor solution at 4000 rpm to coat 20 s on the prepared substrate. After spin coating, transfer to the annealing platform, heat at 100 ℃ for 30 min, and then take out after cooling for use.

Carbon electrode preparation: First, a 10wt% ethyl cellulose chlorobenzene solution was prepared by uniformly stirring ethyl cellulose powder and chlorobenzene solution in a mass ratio of 1:9. Subsequently, 3 g of the aforementioned solution was added to a mixture of 1.2 g graphite and 0.4 g carbon black powder, followed by the addition of 3.8 g chlorobenzene solution to the ball mill at a speed of 300 rpm for a duration of 3 hours. Finally, the resulting carbon slurry was applied onto the surface of the perovskite layer and subjected to heating at 100 °C for 60 minutes.

2.4. Methods for characterization testing

X-ray Diffraction (XRD, Rigaku Ultima IV type) was employed to determine the phase of nano-square $PbTiO_3$ synthesized at various temperatures; Field Emission Scanning Electron Microscopy (FE-SEM) (HITACHI, S-4800) was utilized to observe the morphology of both mesoporous and perovskite layers under different treatment conditions; Transmission Electron Microscopy (TEM) (FEI, TECNAIG2T20) was employed for analyzing the morphology and structure of tetragonal $PbTiO_3$ powder synthesized at different temperatures. Ultraviolet-Visible Absorbance Spectrometer (SHIMADZU UV-2500) was used to analyze the transmittance spectra of mesoporous layers with varying doping fractions and $PbTiO_3$ modified layers with different spin-coating times.

The J-V curve of two batteries incorporating $PbTiO_3$ into TiO_2 mesoporous layer was tested using a Solar Simulator (SOL-2A, 100 mW/cm^2). The Nyquist plot of batteries with differing doping mass fractions were examined by Electrochemical Impedance Spectroscopy (Shanghai Chenhua CHI660E), enabling characterization of parallel impedance in electron-hole pair compounds.

3. Results and discussion

3.1. Enhancing cell performance through $PbTiO_3$-modified TiO_2 mesoporous layer

3.1.1. The analysis of the phase, morphology, and optical properties of $PbTiO_3$ modified layer

$PbTiO_3$ powders are synthesized at different temperatures (150, 180, 200, 220 °C). Firstly, the $PbTiO_3$ powders synthesized at different temperatures are characterized by XRD in order to investigate the effect of synthesis temperature on $PbTiO_3$. Figure 1 exhibits the highest intensity and remain consistent across different synthesis temperatures, and reveals that the diffraction peaks corresponding to angles of 23°, 32°, and 33°. This indicates that they are all tetragonal phase $PbTiO_3$, and they have good crystallinity, which is conducive to a higher spontaneous polarization intensity. [14,15].

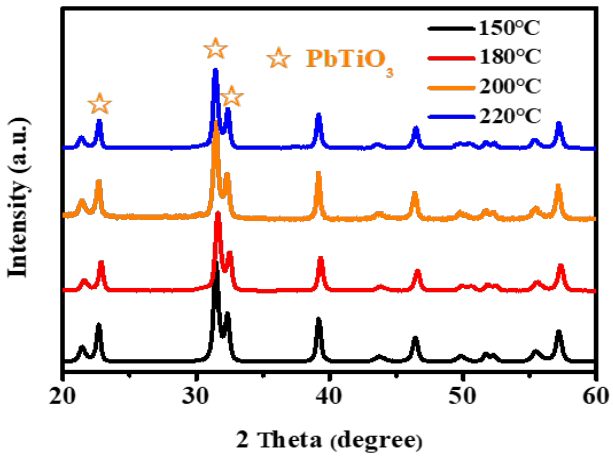

Fig. 1. XRD patterns of $PbTiO_3$ powders synthesized at different temperatures.

Further analysis of the morphology of $PbTiO_3$ synthesized at different temperatures is conducted using TEM characterization. It can be observed that the surface of $PbTiO_3$ particles is characterized by a rough and irregular morphology at 150 ℃ from Figure 2, possibly due to incomplete crystal growth caused by the low temperature [16,17]. At 220℃, the particle size increased further, yet the shape remained irregular with rough edges. Furthermore, the powder particles exhibited significant agglomeration and poor dispersion at varying temperatures.

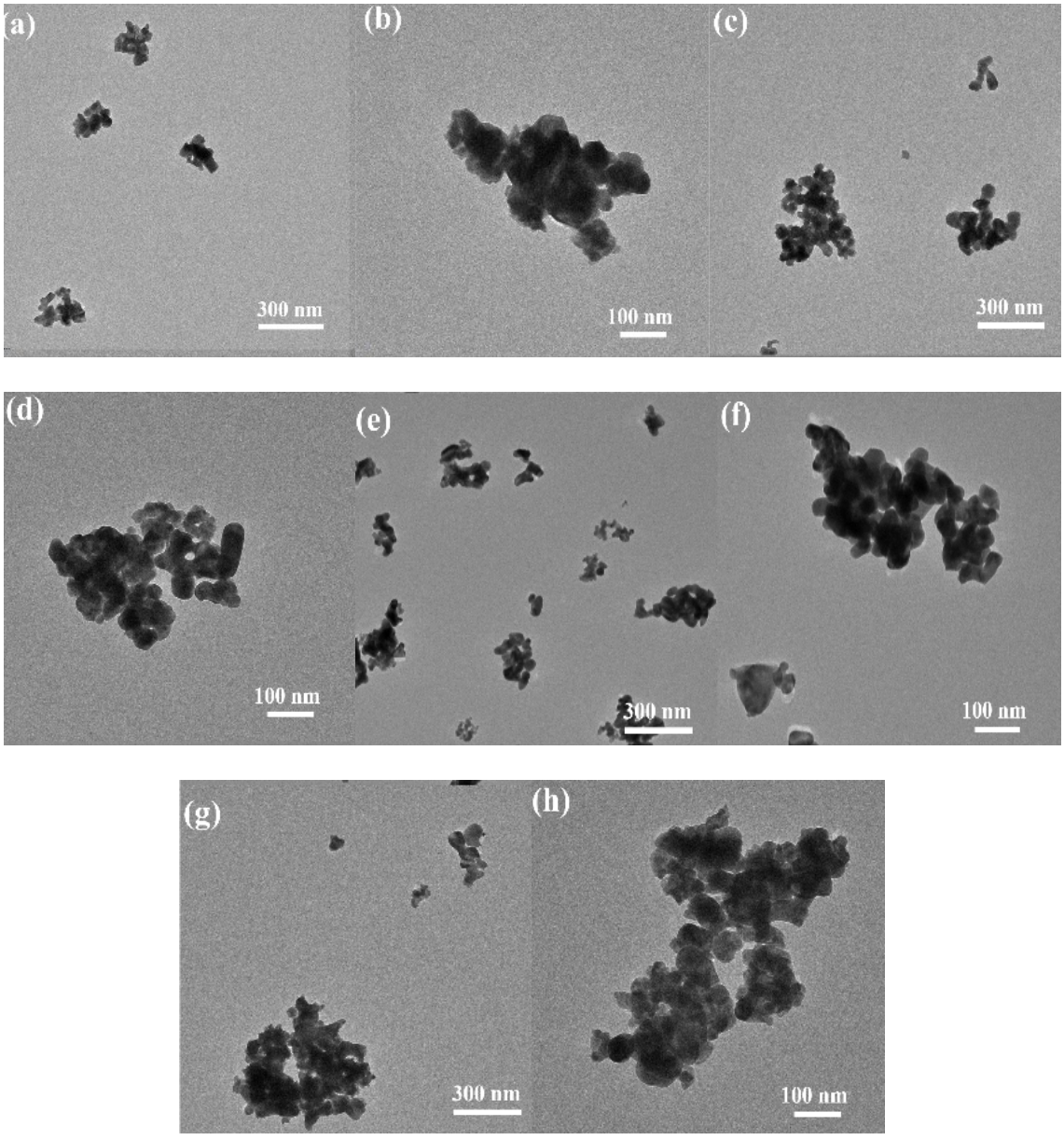

Fig. 2. TEM images of $PbTiO_3$ powder at different synthesis temperatures: (a, b) 150 ℃, (c, d) 180 ℃, (e, f) 200 ℃, (g, h) 220 ℃.

SEM is conducted on the mesoporous layer and perovskite layer before and after modification in order to investigate the effect of $PbTiO_3$ modification on the morphology of the mesoporous layer and perovskite layer. As shown in Figure 3, the coverage rate of the $PbTiO_3$-

modified layer on the TiO_2 mesoporous layer is notably low. This is attributed to the poor dispersibility of $PbTiO_3$ particles, which impairs the uniformity of the dispersion solution of $PbTiO_3$ slurry to be evenly applied on the surface of the mesoporous layer. A comparison of the perovskite layer before and after modification revealed a lower coverage rate of the modified perovskite film This is due to the uneven dispersion of $PbTiO_3$ particles, which impairs the spreading of the perovskite precursor solution on the surface of the mesoporous layer, thereby affecting the light absorption of the perovskite film [18].

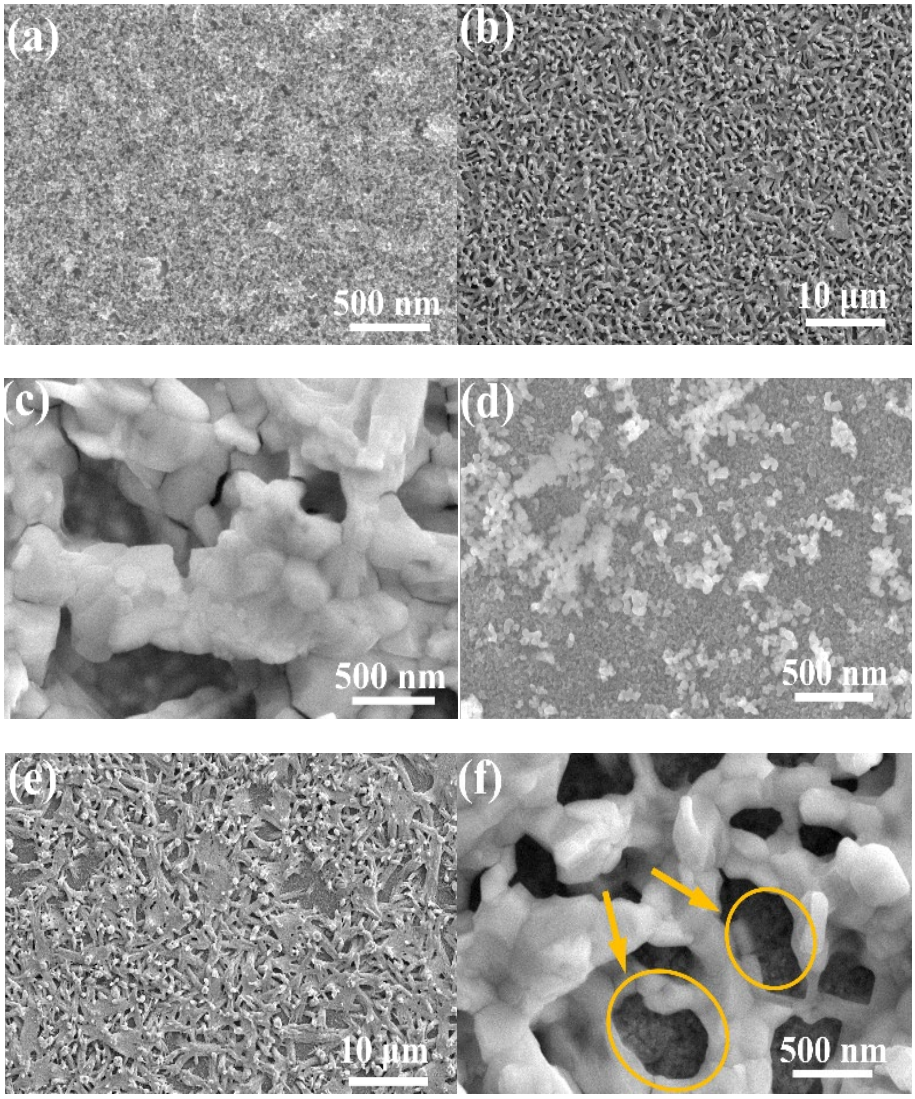

Fig. 3. SEM morphology of the mesoporous layer and perovskite thin film before modification (a-c); SEM morphology of mesoporous layer and perovskite thin film after modification (d-f).

To address the aforementioned issues, the coverage rate of the modified layer is improved by multiple spin-coating of $PbTiO_3$ slurry dispersion on the mesoporous layer, thereby improving the performance of the cell [19,20]. In order to analyze the changes in the mesoporous layer under different spin-coating times, SEM was conducted on the morphology of the mesoporous layer under

different spin-coating times. As shown in Figure 4, with the prolongation of spin-coating times, the modification layer becomes increasingly uniform in density, film coverage increases, and surface roughness diminishes. This indicates that changing spin-coating times can effectively address the issue of the low coverage rate for the modification layer.

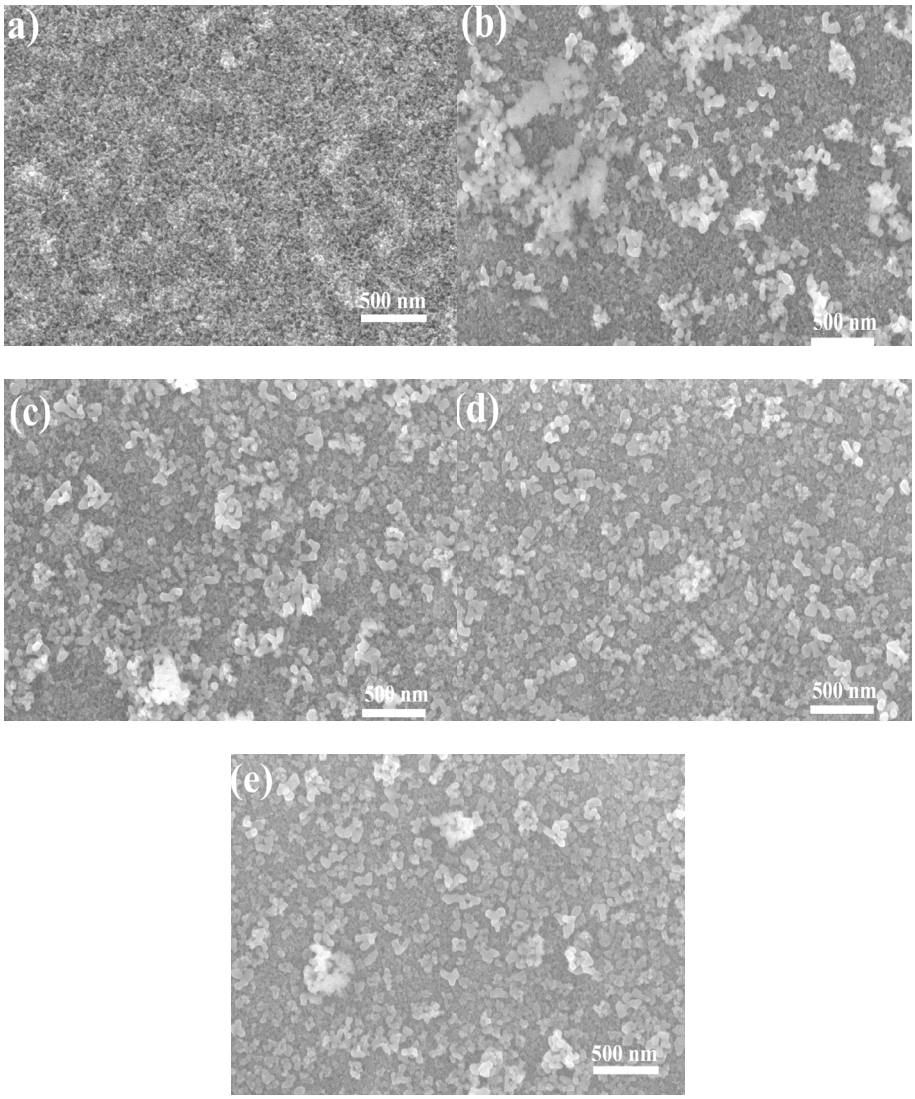

Fig. 4. SEM morphology of the mesoporous layer under different spin-coating times: (a) m-TiO_2, (b) once, (c) twice, (d) three times, (e) four times.

In order to further investigate the feasibility of multiple spin-coating, transmittance characterization tests were carried out on $PbTiO_3$-modified layers with different spin-coating times. As shown in Figure 5, an increase in the number of spin-coats results in the modified layer more uniformly and dense. However, this comes at the cost of a gradual decrease in transmittance, which falls below 50%. This will significantly impede the absorption of visible light by the chalcogenide layer, which in turn will negatively impact the photoelectric conversion efficiency of the cell.

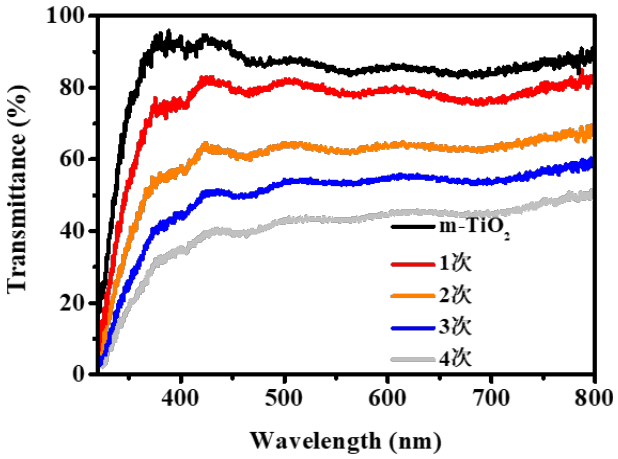

Fig. 5. Ultraviolet-visible transmittance spectra of $PbTiO_3$ modified layers under different spin-coating times.

3.1.2. The effect of $PbTiO_3$ modification on cell performance

J-V curve test is conducted on modified layers of batteries after one spin-coating time. Figure 6 and Table 1 demonstrate that there is minimal variation in open circuit voltage and fill factor between cells with modified layers synthesized at different temperatures. The lowest photoelectric conversion efficiency is observed at 150°C, which may be attributed to incomplete crystal growth leading to poor particle dispersion [21], a low coverage rate of the modification layer, which in turn leads to a decrease in the quality of the perovskite film and affects its absorption of light. The highest short-circuit current density and photovoltaic conversion efficiency is achieved at 180°C, but the improvement was not significant. This phenomenon can be attributed to the inadequate dispersion of $PbTiO_3$ particles and the suboptimal coverage rate of perovskite films following a single spin-coating cycle.

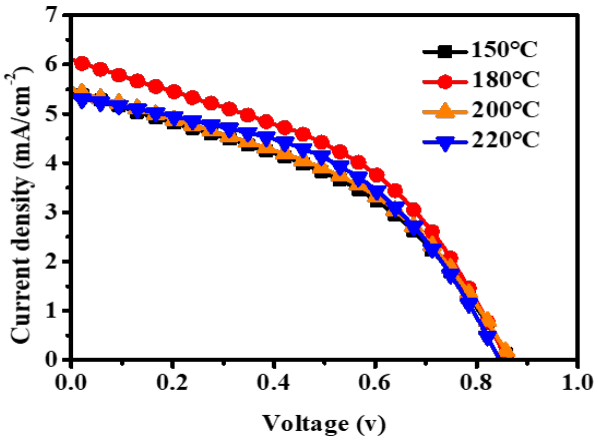

Fig. 6. J-V curves of batteries with $PbTiO_3$ modified layers at different synthesis temperatures.

Table 1. Photoelectric performance parameters of modified layer cells at different synthesis temperatures.

Synthesis temperature(℃)	Voc(V)	Jsc(mA/cm^2)	F_F	PCE(%)
150	0.86	5.46	0.42	1.96
180	0.86	6.10	0.43	2.28
200	0.87	5.49	0.42	2.01
220	0.84	5.34	0.47	2.10

Secondly, J-V curve characterization test is conducted on the modified layers with different spin-coating times. Figure 7 and Table 2 demonstrate that when the spin-coating number is three times, the open circuit voltage of the cell is increased to 0.93 V. This may be attributed to the improvement in the energy level structure between perovskite and TiO_2, as well as the inhibition of the recombination of interface charge carriers, as previously observed in [22]. At the same time, as the spin-coating times increase, the short circuit current density and photoelectric conversion efficiency of the solar cell decrease. This is consistent with the decrease in the transmittance of the modified layer after multiple spin-coating. The decrease in transmittance results in a reduction in the absorption of the perovskite layer by visible light, which in turn leads to a decline in the number of photo-generated charge carriers, resulting in a reduction in the short circuit current density and photoelectric conversion efficiency of the solar cell.

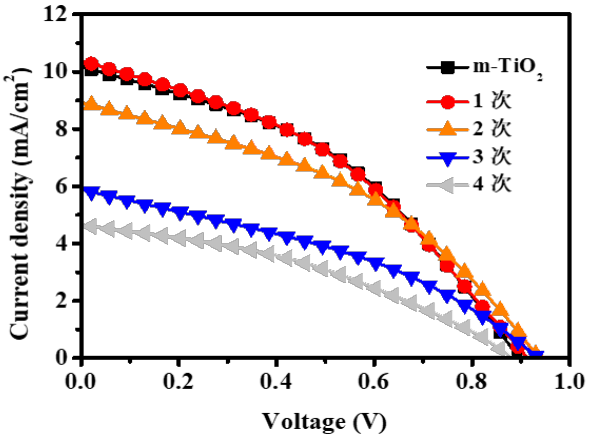

Fig. 7. J-V curves of modified layer cells with different spin-coating times.

Table 2. Photoelectric performance parameters of modified layer cells with different spin-coating times.

Sample paramaters	Voc(V)	Jsc(mA/cm^2)	F_F	PCE(%)
m-TiO_2	0.89	10.17	0.40	3.68
1 time	0.91	10.38	0.39	3.65
2 tines	0.93	8.93	0.40	3.32
3 times	0.93	5.91	0.37	2.02
4 times	0.88	4.65	0.38	1.55

3.2. Enhancing cell performance through $PbTiO_3$-doped TiO_2 mesoporous layer

A $PbTiO_3$-doped TiO_2 mesoporous layer has been incorporated with the objective of enhancing the performance of perovskite solar cells, in order to simultaneously address the issues of low coverage rate and low transmittance,.

3.2.1. Analysis of morphology and optical properties of the TiO_2 mesoporous layer

In order to analyze the influence of $PbTiO_3$ nanoparticles with different mass fractions on the TiO_2 mesoporous layer, SEM characterization tests were first conducted on the morphology of the TiO_2 mesoporous layer doped with different mass fractions of $PbTiO_3$. Figure 8 illustrates that all TiO_2 mesoporous layers doped with different mass fractions of $PbTiO_3$ exhibit loose pores, which is beneficial for the infiltration of perovskite precursor solution into the mesoporous layer to form a dense film. The agglomeration phenomenon of $PbTiO_3$ nanoparticles is not apparent and they exhibit good dispersion. This may be attributed to the fact that TiO_2 nanoparticles impede the agglomeration of $PbTiO_3$ nanoparticles, thereby enhancing their dispersion. Consequently, optimizing the mesoporous layer through doping can diminish the agglomeration phenomenon of $PbTiO_3$ nanoparticles and improve dispersion.

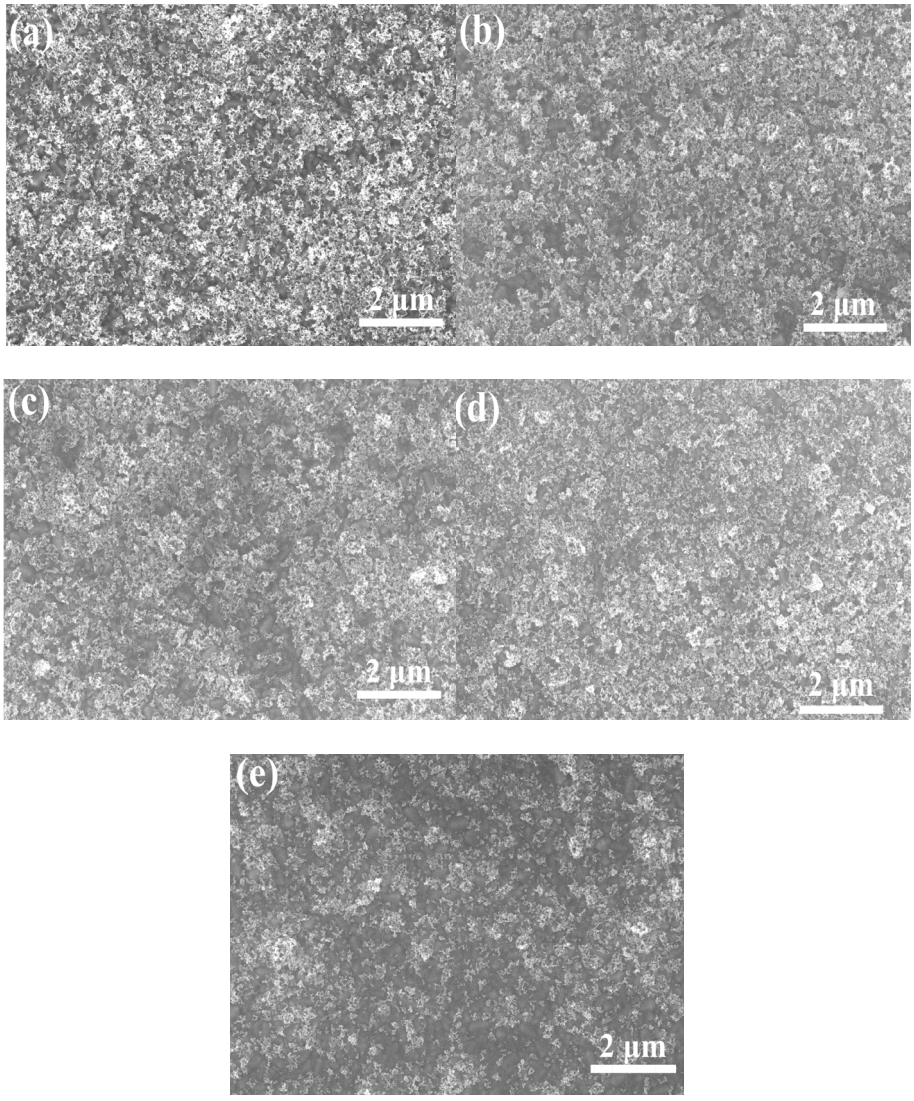

Fig. 8. SEM morphologies of TiO_2 mesoporous layers doped with different mass fractions of $PbTiO_3$: (a) m-TiO_2, (b) 5wt%, (c) 10wt%, (d) 25wt%, (e) 50wt%.

SEM were conducted on the samples in order to analyze the effect of mesoporous layer doping on perovskite films. Figure 9 illustrates that the morphology of the perovskite layer remains unaltered with increasing doping mass fraction, and that all samples exhibit a high degree of coverage. Therefore, doping methods exert a negligible influence on perovskite films, and a high coverage rate is conducive to their absorption of visible light.

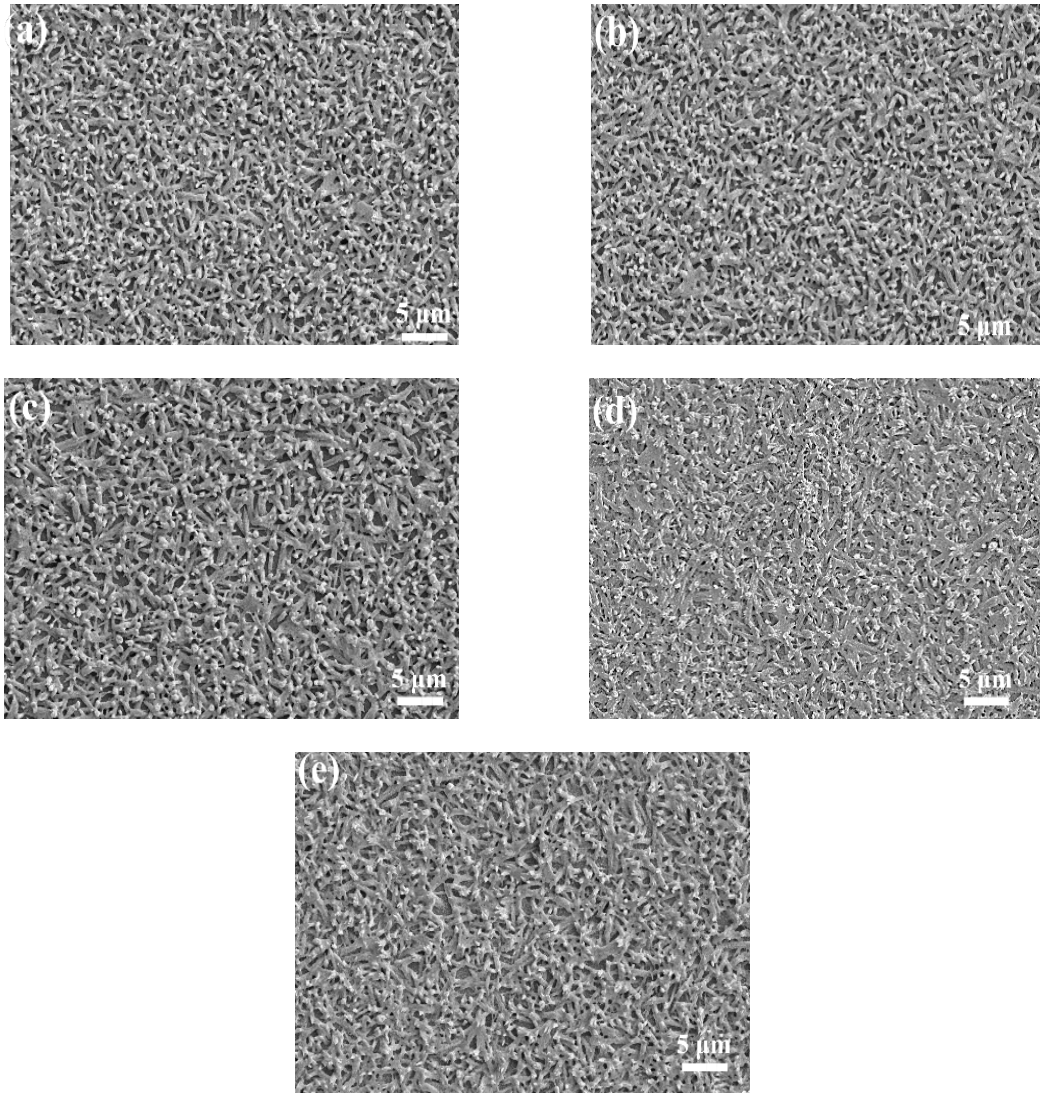

Fig. 9. SEM morphology of perovskite layers of $PbTiO_3$ with different doping mass fractions: (a) m-TiO_2, (b) 5 wt%, (c) 10 wt%, (d) 25 wt%, (e) 50 wt%.

Further UV-visible transmittance spectroscopy characterization test is conducted on mesoporous layers with different doping fractions. Figure 10 illustrates that there is minimal difference in transmittance among mesoporous layers doped with varying mass fractions, with transmittance exceeding 80% within the visible light range of 400-800 nm. The doping methods employed have been found to have a negligible impact on the optimization of the transmittance of mesoporous layers. Furthermore, they can simultaneously address issues related to low coverage rate and low transmittance.

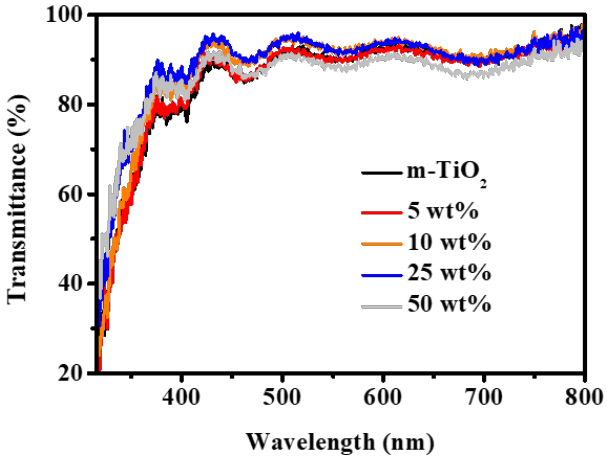

Fig. 10. Ultraviolet visible transmittance spectra of mesoporous layers doped with different mass fractions of $PbTiO_3$.

3.2.2. Effect of $PbTiO_3$ doping on cell performance

J-V curve characterization test is conducted on cells doped with different mass fractions. From Figure 11 and Table 3, it can be observed that when the doping mass fraction is 5wt%, the open circuit voltage increases to 0.93 V, indicating that $PbTiO_3$ in the mesoporous layer can suppress electron-hole recombination at the interface [23]. At a doping mass fraction of 10wt%, the short-circuit current density reaches a maximum of 13.02 mA/cm² and the photovoltaic conversion efficiency also increases to its highest value. The underlying mechanism will be explained in greater detail later in this paper. However, as the doping mass fraction continues to increase to 50wt%, the short-circuit current density decreases, resulting in a decrease in photovoltaic conversion efficiency. In conclusion, the doping mass fraction of 10wt% yields optimal performance for modified cells.

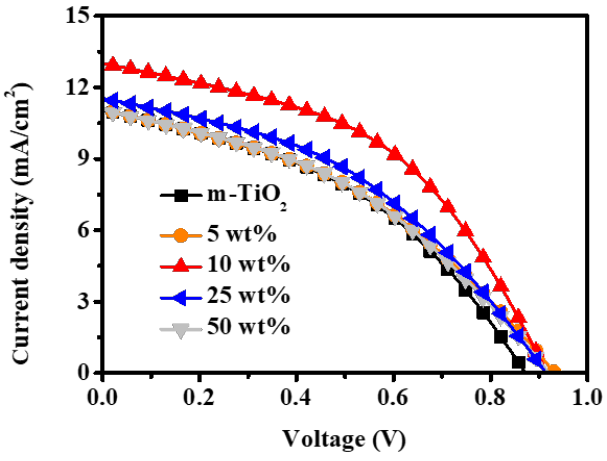

Fig. 11. J-V curves of cells with different doping mass fractions.

Table 3. Photoelectric performance parameters of batteries with different doping mass fractions.

Sample parameters	Voc(V)	Jsc(mA/cm^2)	F_F	PCE(%)
TiO_2	0.87	11.05	0.42	4.04
5wt%	0.93	11.10	0.43	4.43
10wt%	0.92	13.02	0.46	5.51
25wt%	0.92	11.17	0.40	4.11
50wt%	0.90	10.86	0.39	3.81

In order to investigate the reasons for the performance variation of cell devices, electrochemical impedance tests were conducted on batteries with different doping mass fractions. In the Nyquist plot, the impedance in the low-frequency region corresponds to the composite impedance R_{rec} inside the solar cell, which mainly originates from carrier recombination at the interface. Consequently, an increase in Rrec indicates a greater challenge to carrier recombination. Figure 12 illustrates that at a doping mass fraction of 10 wt%, the composite impedance is at its maximum, facilitating electron-hole separation at the interface and improving carrier transport performance at the interface [24], which ultimately enhances the photoelectric conversion efficiency of perovskite solar cells.

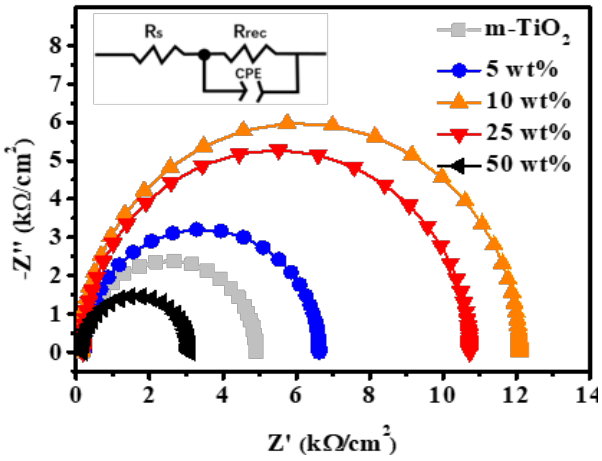

Fig. 12. Nyquist diagram of batteries with different doping mass fractions.

4. Conclusions

The paper utilizes $PbTiO_3$ nanoparticles to optimize the mesoporous layer through two methods of modification and doping. The effects of the modified layer and doping mass fraction on solar cell performance were studied, and the conclusions were as follows.

(1) The $PbTiO_3$ generated by the hydrothermal method has good crystallinity at 180℃, but it tends to aggregate and has poor dispersion at different temperatures. The strong aggregation of $PbTiO_3$ particles, the uneven modification layer and the low thin film coverage rate result in a low photovoltaic efficiency of the solar cell. The use of multiple spin-coating can address the issue of

low coverage rate, however, this approach has the consequence of reducing the light transmittance of the electron transport layer, which in turn results in a reduction in the photovoltaic conversion efficiency of the solar cell.

(2) To address the issues of uniformity and light transmittance in $PbTiO_3$ nanoparticles, the method of doping TiO_2 mesoporous layer with $PbTiO_3$ was adopted. It was found that the dispersion and coverage rate of $PbTiO_3$ nanoparticles were improved significantly without affecting the light transmittance. This can be attributed to the enhanced ability of $PbTiO_3$ in promoting charge carrier separation, leading to the increase in the photoelectric conversion efficiency of the solar cell. The optimal photoelectric conversion efficiency was achieved at a doping mass fraction of $PbTiO_3$ of 10 wt%.

In conclusion, the incorporation of $PbTiO_3$-doped mesoporous layers into perovskite solar cells can enhance carrier separation, thereby improving the efficiency of these devices. This approach represents a superior strategy for optimizing cell performance.

References

[1] A.TH, A. Aiman, J. sustain. dev. energy water environ. syst. 10, 1(2022); https://doi.org/10.13044/j.sdewes.d9.0403

[2] P. Hua, K. Li, G. Chen, J. Cao. Acta Materiae Compositae Sinica, 42, 0(2024).

[3] J.Y. Peng, X. F. Xia, Y. H. Jiang, M. H. Zou, X. F. Wang, Y. Li, M.R. 32, 4027(2018).

[4] J. J. Shi, J. Dong, S. T. Lv, Appl. Phys. Lett. 104, 063901(2014); https://doi.org/10.1063/1.4868101

[5] A. Perez-Tomas, H. Xie, Z. Wang, Sustainable Energy Fuels, 3, 382(2019); https://doi.org/10.1039/C8SE00451J

[6] K. Feng, X. Liu, D. Si, J. Power Sources, 350, 35(2017); https://doi.org/10.1016/j.jpowsour.2017.03.049

[7] Y. H. Chu, L. W. Martin, M. B. Holcomb, Nat. Mater. 7, 478(2008); https://doi.org/10.1038/nmat2184

[8] C. H. Tang, L. B. Li, C. L. Yuan, J. Nanjing Norm. Univ: Nat. Sci. Ed. 3, 41(2005).

[9] V. V. Cherepov, A. N. Kropachev, O. N. Budin, Russ. J. Non-Free MET+, 60, 18(2019); https://doi.org/10.3103/S1067821219010024

[10] L. R. Prado, N. S. de Resende, R. S. Silva, S. M. S. Egues, G. R. Salazar-Banda, Chem. Eng. Process. 103, 12(2016); https://doi.org/10.1016/j.cep.2015.09.011

[11] V. V. Cherepov, A. N. Kropachev, O. N. Budin. Proceedings of Higher Schools Nonferrous Metallurgy, 6, 31(2018); https://doi.org/10.17073/0021-3438-2018-6-31-41

[12] H. Wang, Q. Chen, H. Zhou, J. Mater. Chem. A, 3, 9108(2015); https://doi.org/10.1039/C4TA06394E

[13] W. Li, W. Zhang, R. S. Van, Energy Environ. Sci. 9, 490(2016); https://doi.org/10.1039/C5EE03522H

[14] X. X. Yang, C. D. Cao, L. Erickson, K. Hohn, R. Maghirang, K. Klabunde, Appl. Catal. B-environ. 91, 657 (2009); https://doi.org/10.1016/j.apcatb.2009.07.006

[15] A. Pérez-Tomas, H. B. Xie, Z. W. Wang, H. Kim, I. Shirley, S. Turren-Cruz, Sustainable Energy Fuels, 3, 382(2019); https://doi.org/10.1039/C8SE00451J

[16] Y. F. Liu, Y. N. Lu, S. H. Dai, S. Z. Shi, Powder Technol. 198, 1(2009); https://doi.org/10.1016/j.powtec.2009.09.018

[17] L. J. Che, Y. P. Ding, J. R. Cheng, C. Chen, Z. Y. Meng, MRS Proceedings, 902, 0902(2005); https://doi.org/10.1557/PROC-0902-T10-48

[18] T. Leijtens, B. Lauber, G. E. Eperon, S. D. Stranks, H. J. Snaith, J. Phys. Chem. Lett. 5, 1096(2014); https://doi.org/10.1021/jz500209g

[19] G. E. Eperon, V. M. Burlakov, A. Goriely, H. J. Snaith, Acs Nano. 8, 591(2014); https://doi.org/10.1021/nn4052309

[20] Q. Chen, H. P. Zhou, Z. R. Hong, S. Luo, H. Duan, H. Wang, Y. S. Liu, G. Li, Y. Yang, J. Am. Chem. Soc. 136, 622(2014); https://doi.org/10.1021/ja411509g

[21] T. Li, T. J. Peng, Piezoelectricity & Acoustocptics, 1, 69(2006).

[22] B. Yang, Y. B. Yuan, P. Sharma, S. Poddar, R. Korlacki, S. Ducharme, A. Gruverman, R. Saraf, J. S. Huang, Adv. Mater. 24, 1455(2012); https://doi.org/10.1002/adma.201104509

[23] X. L. Xu, L. B. Xiao, J. Zhao, B. K. Pan, J. Li, W. Q. Liao, R. G. Xiong, G. F. Zou, Angew. Chem. Int. Ed. 59, 19974(2020); https://doi.org/10.1002/anie.202008494

[24] M. I. Khan, A. Mujtaba, M. Fatima, R. Marzouki, S. Hussain, T. Anwar. PCCP, 2024.